

Reconstructing Shapes and Appearances of Thin Film Objects using RGB Images

Yoshie Kobayashi¹, Tetsuro Morimoto², Imari Sato³,
Yasuhiro Mukaigawa⁴, Takao Tomono², Katsushi Ikeuchi¹

¹The University of Tokyo, ²Toppan Printing Co. Ltd.,

³National Institute of Informatics, ⁴Nara Institute of Science and Technology

yoshie.ki@cvl.iis.u-tokyo.ac.jp, tetsuro.morimoto, takao.tomono@toppan.co.jp,
imari.k@nii.co.jp, mukaigawa@is.naist.jp

Abstract

Reconstruction of shapes and appearances of thin film objects can be applied to many fields such as industrial inspection, biological analysis, and archaeologic research. However, it comes with many challenging issues because the appearances of thin film can change dramatically depending on view and light directions. The appearance is deeply dependent on not only the shapes but also the optical parameters of thin film. In this paper, we propose a novel method to estimate shapes and film thickness. First, we narrow down candidates of zenith angle by degree of polarization and determine it by the intensity of thin film which increases monotonically along the zenith angle. Second, we determine azimuth angle from occluding boundaries. Finally, we estimate the film thickness by comparing a look-up table of color along the thickness and zenith angle with captured images. We experimentally evaluated the accuracy of estimated shapes and appearances and found that our proposed method is effective.

1. Introduction

Reconstructing the shapes and appearances of real objects is an important issue in the computer vision and computer graphics fields. Several of the current reconstruction methods issue reflectance properties which describes the reflection between reflected and incoming light. However, objects in the real world have quite a few different reflectance properties such as diffusion, specularity, isotropy, anisotropy, scattering, refraction, and interference. Among these, interference has been less explored due to difficult elements such as dramatically varying color along the lighting and viewing directions. Such interference effects are observed on the thin layer over object surfaces such as laminated film, soap bubbles, and oil film. Although it can be

difficult, thin film modeling is applied in many areas such as industrial inspection, biological analysis, and archaeological research.

In computer graphics, several methods have shown that a physical model of interference can represent appearances well. However, this type of a model requires optical parameters (refractive index and film thickness) to determine appearances. In optics fields, there are several methods to estimate optical parameters, such as the refractive index and film thickness of a planar object. Interference spectroscopy[13] and ellipsometry are representative methods. Kitagawa[11, 10] proposed an image-based method, that utilizes RGB values along the film thickness, but this method requires a known refractive index. Some applications such as archaeological applications require the thickness of a curved surface to be measured, meaning that they cannot be applied to non-planar surfaces. Kobayashi et al.[12] proposed a method for thin film objects that have a complicated shape. The problem with this method, though, is that it needs spectral images for the analysis, and thus the data dimensionality becomes high due to the high volume of memory and computational complexity required.

In this paper, we propose a novel method to estimate the shapes and film thickness of an object with thin film layers by using only RGB images. The shape of an object is estimated on the basis of polarization and intensity change along the zenith angle. From the observed color and obtained object shape, the method compares color change of a simulated result with the observed image, and then determines film thickness from the closest color.

The three main contributions of this work are as follows. First, while conventional methods use spectral sensors, we use only a commercial available digital camera, resulting in less data to be processed. Second, our method can obtain both the shape and film thickness of a target object. Third, we have developed a novel measurement apparatus that can

capture the whole reflectance of a thin film at once.

The proposed method comes with several assumptions. First, the target object must have a single thin film on its surface. Second, the object surface must be geometrically smooth and closed with no self-occlusion. This assumption is necessary to disambiguate azimuth angles. If a rough shape of the object is known, this assumption is not necessary. Third, the refractive index of the object must be known in order for the polarization to narrow down candidates of the zenith angle. Fourth, there must be no (or very little) inter reflection or subsurface scattering. Finally, the observed light must be only interference reflection from thin film, because interference light can be observed when the observed angle is the same as the incident angle on the surface normal.

The rest of this paper is as follows. In Section 2, we discuss several existing methods of reconstructing shapes and appearances for various reflection properties. In Section 3, we propose our method of estimating the shapes of thin film objects on the basis of polarization analysis. In Section 4, we describe the representation of thin film appearances in RGB space, and in Section 5, we introduce the measurement equipment of our method, the procedure of the shape estimation, and the method for estimating film thickness. In Section 6, we present experimental results and discuss the accuracy of our method. We conclude in Section 7 with a brief summary and mention the future work.

2. Related Work

Various methods to acquire the appearances of objects in the real world have been proposed. In computer vision fields, appearances are defined by a bidirectional reflection distribution function (BRDF) that represents reflectance along the view and light directions. Holroyd et al. [7] and Dana et al. [2] constructed a BRDF look-up table in which they controlled the illumination and view directions by positioning the light, sensor, and sample sequentially. Mukaigawa et al. [17] and Dana et al. [3] have used an ellipsoidal mirror to measure the reflection of all directions at once. However, these methods are centered on reflection, which does not dramatically vary the appearance. It is thus difficult to apply these methods to thin film objects.

There are several methods to estimate shapes and appearances simultaneously. A representative method is the photometric stereo [4], which is applied to various reflectance properties such as diffusion, specularity, isotropy, and anisotropy. This method usually estimates shapes while fitting a reflectance model with captured images. However, when the reflectance of transparent objects is too complicated, this method does not work well. Several methods [22][19][14][15][16] have been proposed to estimate the shapes of transparent objects using polarization.

In computer graphics, there are several methods to render

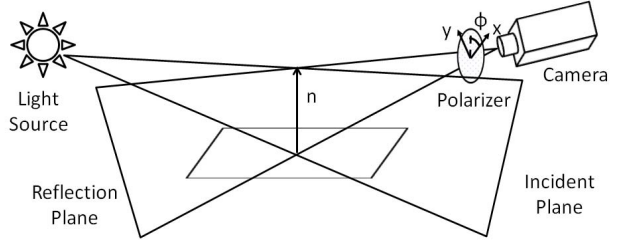


Figure 1. Relation between incident plane and azimuth angle. x and y are coordinates in camera view. ϕ is rotation angle at perpendicular polarization.

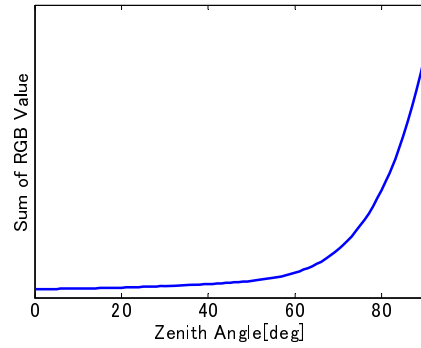


Figure 2. Sum of RGB values along zenith angle. The refractive index of thin film is 1.36 and that of bottom layer is 1.6. Film thickness is 400 nm. Sensitivity of the camera is EOS 5D [9]

structural color caused by thin film, multiple films, refraction, and diffraction grating. Hirayama et al. [6, 5] have rendered multi-film interference focusing on a physical model while Sun et al. [21, 20] models the micro-structure of CDs precisely and reconstruct it realistically. Using the model of refraction among water droplets, Sadeghi et al. [18] have rendered a rainbow the same as a real images. Cuypers et al. [1] uses the Wigner distribution function to model diffraction grating. They compare this model with reflectance from objects in the real world and show that it can represent the appearance as precisely as a physical model. Using a physical model, these methods can represent appearances well, but the model parameters need to be set manually, which means we need to estimate the parameters of the physical model in order to reconstruct the thin film appearance well.

3. Shape Estimation

In this section, we propose a shapes reconstruction method based on polarization and reflectance intensity analysis of thin film objects. The polarization and reflectance intensity are explained in the following.

3.1. Polarization

Light has the characteristics of an electromagnetic wave. The polarization of reflected light can be divided by parallel

and perpendicular polarization. The parallel polarization is parallel light along the incident plane and the perpendicular polarization is vertical light along the incident plane. As shown in Fig. 1, the azimuth angle is vertical along the incident plane and the perpendicular polarization is parallel to the azimuth angle.

3.2. Zenith Angle

We focus on two features to estimate zenith angles. The first feature is the degree of polarization (DOP), which can narrow down candidates to two zenith angles. The second one is the intensity of perpendicular polarization, which monotonically increases as shown in Fig. 2. In this section, we propose a method to estimate zenith angles using these two features.

When the polarizer is rotated, the observed intensity is changed along the rotating angle. We can obtain the degree of polarization (DOP) by using the maximum and minimum intensities among polarized images, as shown in Fig. 3. The refractive indices are the same as Fig. 2. DOP is represented as

$$\rho = \frac{I_{max} - I_{min}}{I_{max} + I_{min}} \quad (1)$$

The I_{max} and I_{min} can be theoretically defined as amplitude of Fresnel reflection and transmittance as

$$\begin{aligned} I_{max} &= I_s \\ &= (R_s(t) + T_s(t)R_s(b)T_s(b))I \end{aligned} \quad (2)$$

$$\begin{aligned} I_{min} &= I_p \\ &= (R_p(t) + T_p(t)R_p(b)T_p(b))I \end{aligned} \quad (3)$$

where $R_s(t)$, $R_p(t)$ are the reflections of the top layer, $R_s(b)$, $R_p(b)$ are the reflections of bottom layer, $T_s(t)$, $T_p(t)$ are the transmittance coefficients of the top layer, and $T_s(b)$, $T_p(b)$ are the transmittance coefficients of the bottom layer.

A schematic diagram of thin film is shown in Fig. 4. The amplitude of the Fresnel reflection and transmittance at the top layer are represented as Eq. (4), (5), (6), and (7). In the case of the bottom layer, the equations can be similar to the top layer's equations. n_1 , n_2 , and n_3 are the refractive indices of the incoming medium, thin film, and outgoing medium, respectively. θ_1 is zenith angle. θ_2 is refracting angle. θ_3 is angle of outgoing light transmitting the thin film. In our method, we assume that the incoming medium is air, so $n_1 = 1.0$.

$$R_s(t) = \left| \frac{n_1 \cos \theta_1 - n_2 \cos \theta_2}{n_1 \cos \theta_1 + n_2 \cos \theta_2} \right|^2 \quad (4)$$

$$R_p(t) = \left| \frac{n_2 \cos \theta_1 - n_1 \cos \theta_2}{n_2 \cos \theta_1 + n_1 \cos \theta_2} \right|^2 \quad (5)$$

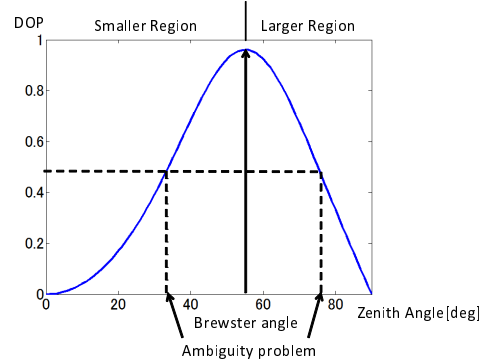


Figure 3. Degree of polarization. Refractive indices of thin film and bottom layer are 1.36 and 1.6, respectively.

$$T_s(t) = \frac{\tan \theta_1}{\tan \theta_2} \left| \frac{2 \sin \theta_2 \cos \theta_1}{\sin(\theta_1 + \theta_2)} \right|^2 \quad (6)$$

$$T_p(t) = \frac{\tan \theta_1}{\tan \theta_2} \left| \frac{2 \sin \theta_2 \cos \theta_1}{\sin(\theta_1 + \theta_2) \cos(\theta_1 - \theta_2)} \right|^2 \quad (7)$$

Here, we can calculate the DOP along the zenith angle if we know the refractive index of the thin film and bottom layer.

As shown in Fig. 3, the DOP has two solutions across the Brewster angle. In Fig. 3, the vertical axis is the value of DOP and the horizontal axis is the zenith angle from 0 to 90 degrees. To solve before the ambiguity, we came up with the following method. We can divide by two regions, e.g., a larger region and a smaller region. The larger region has a larger angle than the Brewster angle and the smaller region has a smaller one. The intensity of perpendicular polarization can be calculated from Eqs. (2), (4), and (6). When the intensity becomes larger than that of the Brewster angle, we can determine that region as the larger region and can then detect the zenith angle in the larger region. The reverse is true when the intensity is smaller than that of the Brewster angle.

3.3. Azimuth Angle

We can estimate azimuth angles by using perpendicular polarization. We detect rotation angles observing perpendicular polarization and estimate azimuth angles. When the polarizer is rotated, the intensity of captured images is changed from bright to dark among a 180° polarizer rotation. As mentioned in the previous section, azimuth angle is parallel to perpendicular polarization. Therefore, the rotation angle is equal to azimuth angle when we observe maximum intensity. However, there are two maximum intensities. If we define one angle as ϕ , the other one becomes $\phi + 180^\circ$. We can solve this ambiguity by using the occluding boundaries of the target object.

Then, we assume that surface normal directs outwards. When the occluding boundary is closed, the integrated value

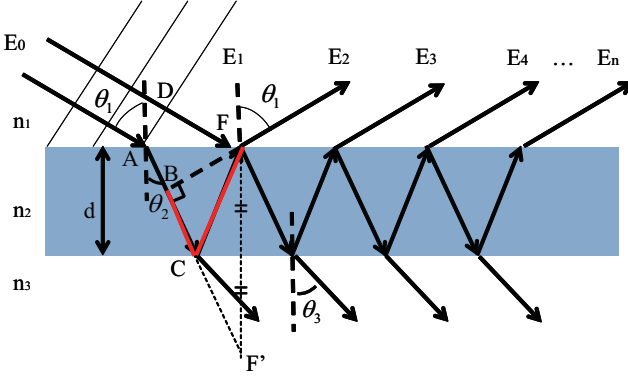


Figure 4. Schematic diagram of thin film interference. n_1 , n_2 and n_3 are refractive indices of incoming medium, thin film and outgoing medium respectively. θ_1 is zenith angle. θ_2 is refracting angle. θ_3 is angle of outgoing light transmitting the thin film.

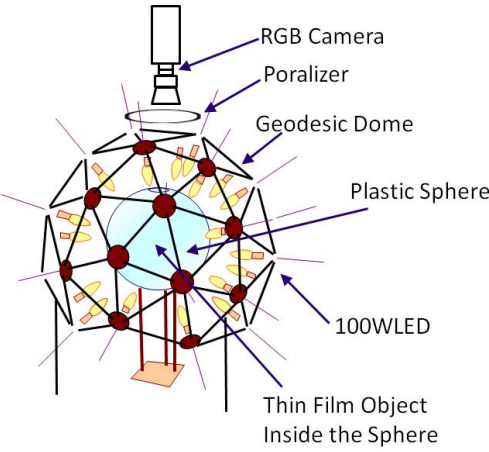


Figure 5. Proposed measurement equipment of our method. We put an LED light on top of an icosahedron with a white plastic sphere inside it to create an omnidirectional light environment. We also put an RGB camera on top of the sphere and polarizer.

of surface normal in a small region becomes 0 [8] as

$$\iiint_C f(x, y, z) dx dy dz = 0 \quad (8)$$

where C is the small region area on target objects. We estimate azimuth angles of whole objects with the following steps.

1. Estimate azimuth angles of occluding boundaries assuming that all azimuth angles of boundaries direct outwards.
2. For estimating azimuth angles of inside area, we expand the estimated result to near the boundaries in the first step. Then the estimated azimuth angle should be satisfied Eq. (8).
3. Apply the second step to the rest of all pixels.

4. Appearance of Thin Film Reflectance in RGB Space

In this section, we describe the appearance of thin film object in RGB color space. Our method can be used with a regular digital camera. Observed RGB values are represented by integration of observed spectra. The observed spectrum is a multiplication of the camera sensitivity, reflectance, and illumination spectrum in Eq. (9).

$$I_{RGB} = \int S_{RGB}(\lambda) R(\lambda) E(\lambda) d\lambda \quad (9)$$

I_{RGB} is observed RGB value. $S_{RGB}(\lambda)$ is camera sensitivity function. $R(\lambda)$ and $E(\lambda)$ are reflectance and illumination spectra, respectively.

The reflectance spectra of thin film $R(\lambda)$ is defined by

$$R(\lambda) = \left| \frac{r_{12} + r_{23}e^{i\Delta}}{1 + r_{23}r_{12}e^{i\Delta}} \right|^2 \quad (10)$$

r_{12} and r_{23} are Fresnel coefficients and represented by Eqs. (11), (12), (13), and (14) for perpendicular and parallel polarization.

$$r_{12}^s = \frac{n_1 \cos \theta_1 - n_2 \cos \theta_2}{n_1 \cos \theta_1 + n_2 \cos \theta_2} \quad (11)$$

$$r_{12}^p = \frac{n_2 \cos \theta_1 - n_1 \cos \theta_2}{n_2 \cos \theta_1 + n_1 \cos \theta_2} \quad (12)$$

$$r_{23}^s = \frac{n_2 \cos \theta_2 - n_3 \cos \theta_3}{n_2 \cos \theta_2 + n_3 \cos \theta_3} \quad (13)$$

$$r_{23}^p = \frac{n_3 \cos \theta_2 - n_2 \cos \theta_3}{n_3 \cos \theta_2 + n_2 \cos \theta_3} \quad (14)$$

Δ in Eq. (10) is phase difference.

$$\Delta = \frac{2\pi\varphi}{\lambda} \quad (15)$$

where φ is an optical path difference determined by a distance between point A and point F in Fig. 4. The distance is $ACF - DF$. Considering a light going into a medium with refractive index n_2 , the light speed in thin film is defined by n_2c , where c is the light speed in the air. Therefore, the optical path difference becomes $n_2ACF - n_1DF$. In Fig. 4, n_1 is the refractive index in the air, so $n_1 = 1$. The optical path difference DF is equal to n_2AB .

$$n_2ACF - DF = n_2BCF \quad (16)$$

The optical path difference BCF is equal to $BCF' = 2d \cos \theta_2$ since F' is symmetrical point F .

$$\varphi = n_2BCF = 2dn_2 \cos \theta_2 \quad (17)$$

Therefore, in Eq. (10), a zenith angle θ_1 , refractive indices n_2 , n_3 , and film thickness d are important parameters for appearances. In our case, only film thickness d is unknown.

5. Implementation

In this section, we propose the novel measurement equipment and, explain how this equipment is used to estimate both the shape and film thickness.

5.1. Measurement Equipment

Fig. 5 shows the measurement equipment for polarized images of thin film objects. This equipment consists of a geodesic dome, LED light, white plastic sphere as a diffuser, a RGB camera, and a linear polarizer. The spectrum of LED light is preferable because it is similar to the spectrum of daylight illumination. We use a Canon EOS 5D Mark2 as a conventional RGB camera, the sensitivity of which has been measured by Kawakami et al.[9].

Using this equipment, we can capture appearances of an object under omnidirectional illumination, since the interference light can be observed when the incident angle of light and the observed angle on normal is the same. In our equipment, we place the LED lights at the vertex of the geodesic dome and a plastic sphere for diffusing light around the target object.

5.2. Procedure of Shape Estimation

Fig. 6 shows the procedure to estimate the shape of thin film objects. The estimation method is roughly divided into three steps. First, we capture polarized images by rotating the polarizer from 0 to 180 degrees. The latter two steps, which are performed independently of each other, are for estimating the zenith and azimuth angles.

First, we store the pixel intensities in the captured image sequence. Second, we detect the maximum and minimum intensities in the captured image sequence and calculate the DOP in each pixel. Third, using the calculated DOP, we determine two candidates of the zenith angle. Finally, we determine the zenith angle using Section 3.2.

The azimuth angle estimation is as follows. First, we detect the angle of maximum intensity in each pixel of the captured image sequence. Next, the azimuth angles in the whole region can be estimated using the method in Section 3.3.

5.3. Procedure for Appearance Reconstruction

In this section, we propose a method to estimate film thickness. When we know the refractive index of a thin film, we can simulate the appearance along the zenith angle and film thickness by using Eq. 10. As shown in Fig. 7 whose optical parameters are the same as in Fig. 2, the appearance can be determined uniquely for the zenith angle and the film thickness. However, we can observe a similar appearance repeatedly along the film thickness. When we input the appearance at a certain zenith angle and take the least square minimum between observed appearance and

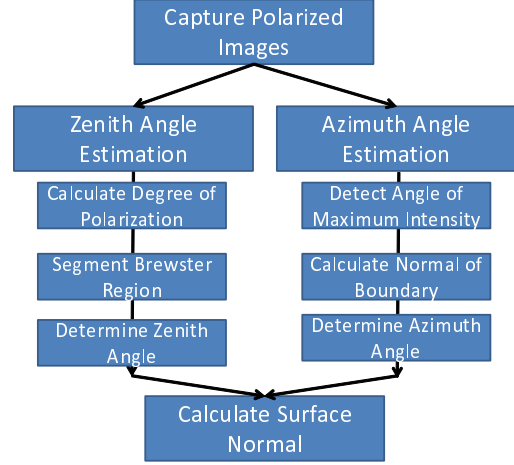


Figure 6. Process flow of the shape estimation

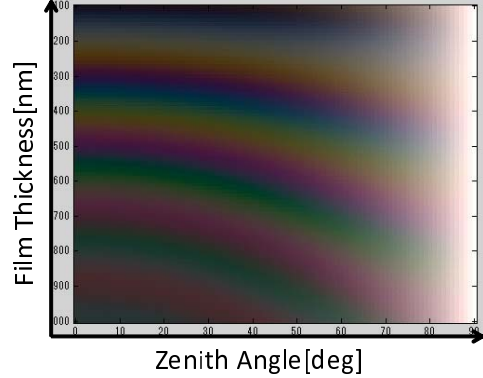


Figure 7. Simulated appearance along zenith angle and film thickness. Zenith angle is from 0 to 90 degrees. Film thickness is from 100 nm to 1000 nm.

simulated appearance, we can find the local minimum along the film thickness. Therefore, we need to know the rough range of the film thickness in advance.

6. Experiment

In this section, we investigate the validity of our method by simulation. We also verify the effectiveness of our method with real objects.

6.1. Simulation

We investigated the accuracy of the film thickness estimation and found that the accuracy of azimuth angles depends on the detection accuracy of the rotation angle of the polarizer. The accuracy of the rotation angle has previously been evaluated [19][14][15], so in this section, we examine only the accuracy of the film thickness estimation. We use reflectance spectra measured with a spectrometer as input data. We put the target object and light source on a rotation table and changed the zenith angle from 10 to 50 degrees

by 5-deg increment. The material used for the thin film is MgF_2 with a refractive index of 1.36. The material of the bottom layer is a polyethylene terephthalate(PET) film with a refractive index of 1.6. The ground truth of film thickness is 630 nm. Tab. 1 shows the estimated film thickness and RMSE between measured reflectance and reflectance model with ground truth optical parameters. The average error is 6.56 nm. At 15 and 50 degrees, the error is over 10 nm.

Table 1. Estimated Thickness and RMSE of Measured Reflectance

Zenith angle [deg]	Estimated thickness [nm]	RMSE[%]
10	629	1.20
15	618	1.44
20	630	1.05
25	632	0.87
30	628	0.99
35	624	1.45
40	626	1.18
45	639	1.13
50	661	1.31

6.2. Measurement of Real Object

In this section, we demonstrate the measurement of a few real objects using our equipment. For this experiment, we used a cylindrical object, and a quadrangular pyramid button with MgF_2 evaporated on their surfaces. The bottom layer of the cylindrical object is PET film with a refractive index of 1.6 and film thickness of 400 nm. The planar thin film was rolled up onto the cylindrical object.

The quadrangular pyramid object is made of acrylonitrile butadiene styrene (ABS) resin with a refractive index of 1.5. It had MgF_2 directly evaporated on its surface, the film thickness of which was 630 nm. Physical vapor deposition is generally used for planar objects, but there is no guarantee that film thickness is evaporated uniformly on non-planar objects. However, our method can measure spatial normal and thickness on a non-planar object.

First, we show the estimated results of the zenith angle in Figs. 8 . Figs. 8 . (b) shows the estimated zenith angle. The middle area of Figs. 8 is facing the hole in the plastic sphere of the geodesic dome. We captured images thorough this hole and then obtained no solution in this area.

Second, we show the estimated surface normal and its error in Figs. 9 . The top row of Figs. 9 shows the results of the cylindrical object. The average error was 4.48 degrees. The bottom row of Figs. 9 shows the results of the quadrangular pyramid object. The average error was 2.82 degrees. Figs. 9.(c) shows the errors of angles between the ground truth and estimated surface normals.

Third, Figs. 10 show the results of estimated film thickness. The thickness is around 400 nm for the cylindrical object. However, the thickness of the quadrangular pyramid object varied greatly from 400 nm to 690 nm.

Finally, we show the reconstructed appearance images using our method in Figs. 11 . We evaluated the color difference between captured and reconstructed images. The color difference is defined by Eq. (18) in CIE Lab color space. CIE defined the difference level of human perception between two colors.

$$\Delta = \sqrt{\Delta L^2 + \Delta a^2 + \Delta b^2} \quad (18)$$

The color difference of the cylindrical object, 0.64, is perceived as “Slight”. The color difference of the quadrangular pyramid, 3.0, is perceived as “Noticeable” .

6.3. Discussion

In this section, we discuss the errors of the simulation and experiment with real objects. First, we examine the thickness error in the simulation. We calculate RMSE between measured reflectance spectra and spectra with ground truth film thickness. RMSE became larger at 15 and 50 degrees, as shown in Table 1 . This result indicates that the input reflectance is affected by noise.

We examine the errors of the experiment with real objects. First, we consider that the error is caused by zenith angle error and azimuth angle error. The difference between the zenith angle error in Figs. 8 and surface normal in Figs. 9 is almost the same. Hence, the error of azimuth angle is almost zero.

Second, Fig. 12 shows reflectances of perpendicular and parallel polarization along the zenith angle. The optical parameters are the same as Fig. 2 . We consider that the error of zenith angles is caused by the noise in input intensity in the lower angle, as shown in Fig. 12 . In this area, the difference in angle estimation is quite small with a certain intensity difference. This indicates that the estimated zenith angle is sensitive to noise.

Third, we can recognize the smooth spatial thickness of both objects, but we do not know the ground truth of thickness in Figs. 10 . Physical vapor deposition is subject to evaporating thin film: the thinner it is and the farther away from center of the target objects it is. Our results confirm this effect.

Finally, we discuss the difference of the reconstructed appearances in Figs. 11 . In our method, we were able to estimate the optical parameters of thin film, such as spatial normal and spatial thickness by a regular digital camera. As shown in Figs. 11 , the complex appearance changes of thin film can be represented. In the future, we will discuss how to improve our method for more accurate reconstruction.

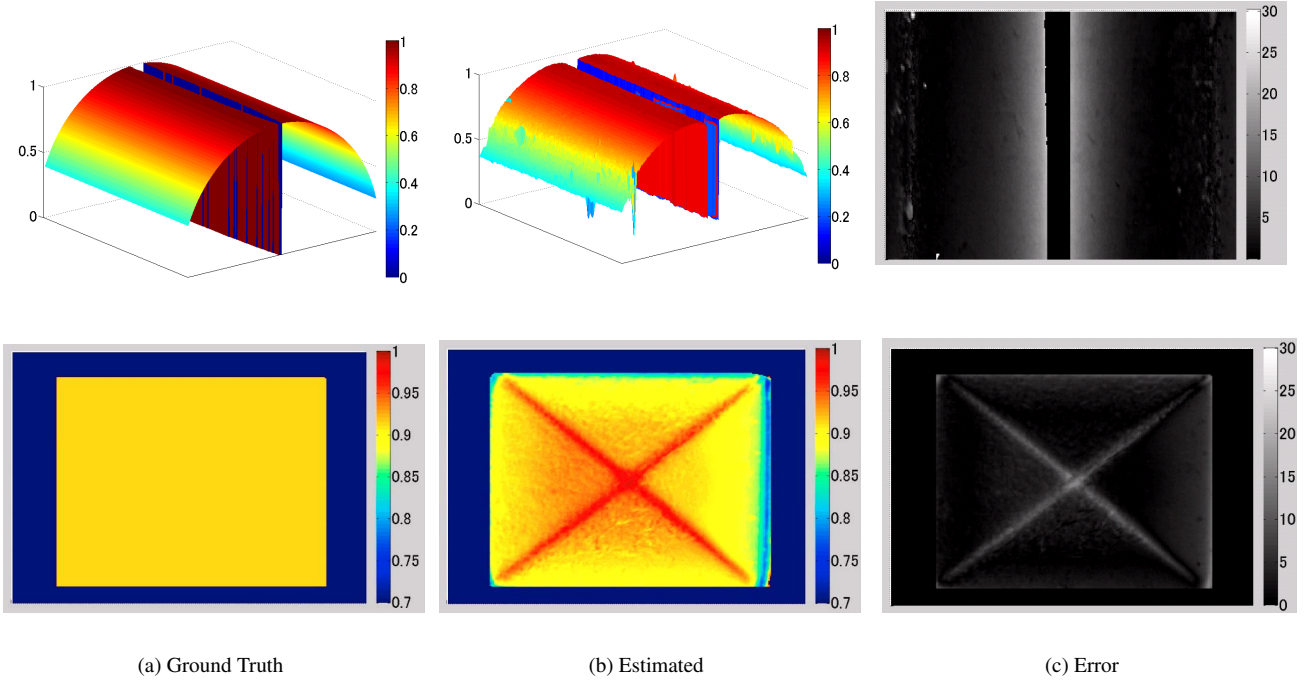


Figure 8. Estimated results of zenith angle. (a) Ground truth in polar coordinates. (b) Estimated zenith angle in polar coordinates. (c) Estimation error in degrees.

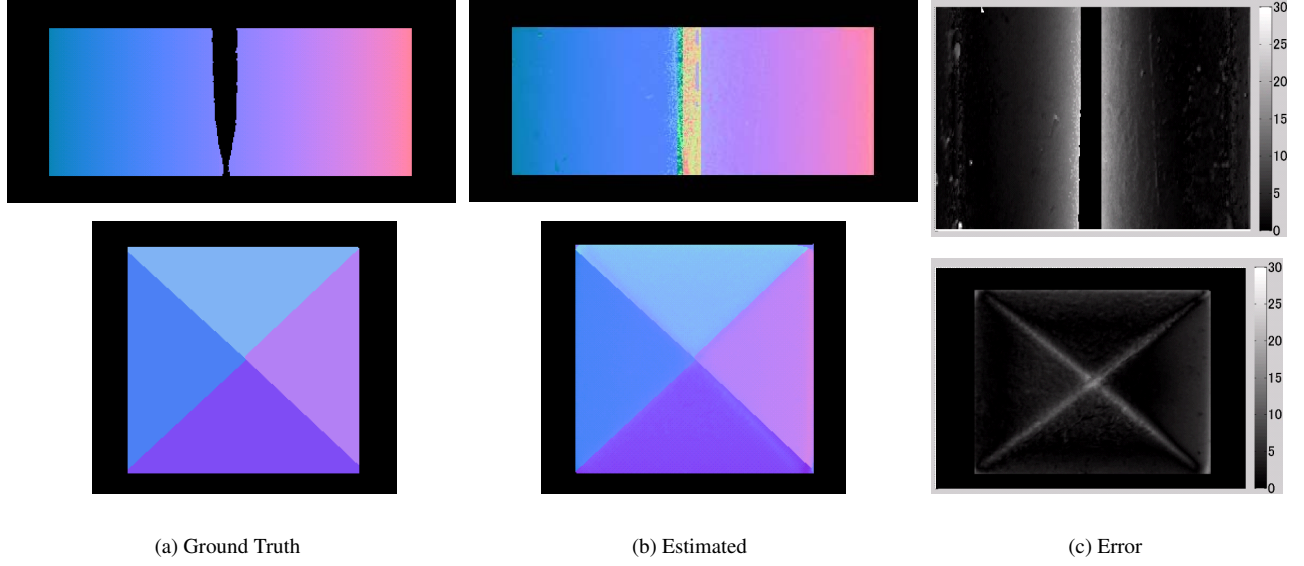


Figure 9. Estimated results of surface normal. (a) Ground truth. (b) Estimated surface normal. (c) Estimation error in degrees.

7. Conclusion

We proposed a novel method to estimate the shape and appearance of thin film objects using RGB images. By our method, we can determine both the shape and thickness of thin film objects using a regular digital still camera and measure the thin film object easily. We also developed the

measurement equipment to capture whole reflectance images of thin film objects at once. In this paper, our focus was thin film objects with a single layer, but theoretically our method can also be applied to the reconstruction of the shape of multi-layered thin film objects. At the moment, it is difficult to estimate film thickness at each layer of a multi-layered thin film. In the future, we will extend our method

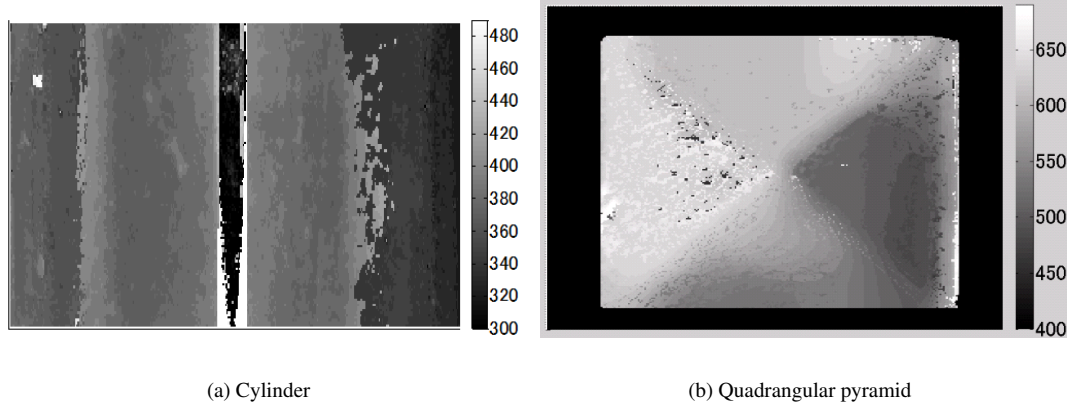


Figure 10. Estimated results of film thickness.

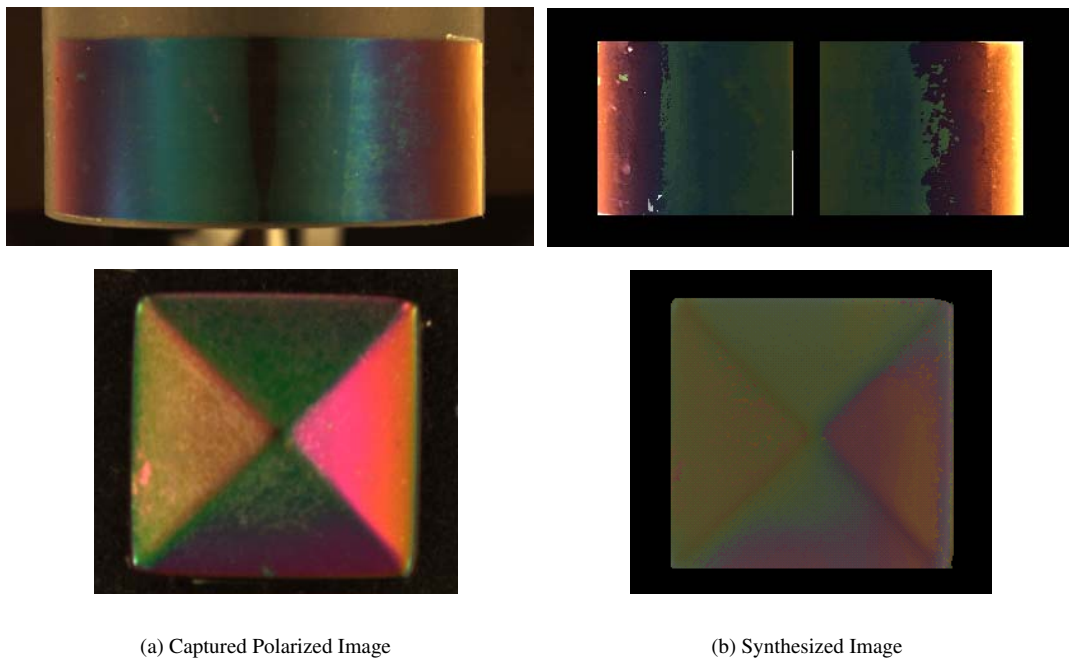


Figure 11. Captured polarized image and reconstructed image with estimated shapes and film thickness.

to model multi-layered thin film objects.

Acknowledgement

This research was supported in part by Grant-in-Aid for Scientific Research on Innovative Areas (No.15H05918) from MEXT, Japan

References

- [1] T. Cuyvers, T. Haber, P. Bekaert, S. B. Oh, and R. Raskar. Reflectance model for diffraction. *ACM Trans. Graph.*, 31(5):122:1–122:11, Sept. 2012.

- [2] K. J. Dana, B. van Ginneken, S. K. Nayar, and J. J. Koenderink. Reflectance and texture of real-world surfaces. *ACM Trans. Graph.*, 18(1):1–34, Jan. 1999.
 - [3] K. J. Dana and J. Wang. Device for convenient measurement of spatially varying bidirectional reflectance. *J. Opt. Soc. Am. A*, 21(1):1–12, Jan 2004.
 - [4] S. Herbort and C. Wölfler. An introduction to image-based 3d surface reconstruction and a survey of photometric stereo methods. *3D Research*, 2(3), 2011.
 - [5] H. Hirayama, K. Kaneda, H. Yamashita, and Y. Monden. An accurate illumination model for objects coated with multi-layer films. *Computers and Graphics*, 25(3):391–400, 2001.
 - [6] H. Hirayama, Y. Yamaji, K. Kaneda, H. Yamashita, and Y. Monden. Rendering iridescent colors appearing on natural objects. In *Computer Graphics and Applications*, 2000,

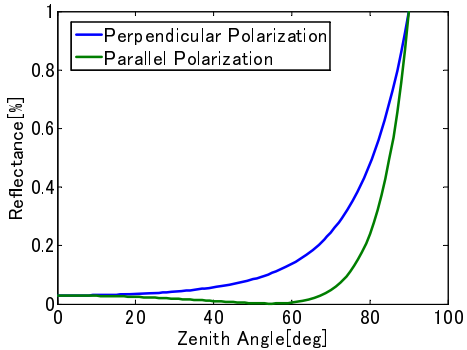


Figure 12. Reflectance of perpendicular and parallel polarization. Reflectance is the percentage of reflected light from an object.

- Proceedings. The Eighth Pacific Conference on*, pages 15–433, 2000.
- [7] M. Holroyd, J. Lawrence, and T. Zickler. A coaxial optical scanner for synchronous acquisition of 3d geometry and surface reflectance. *ACM Trans. Graph.*, 29(4):99:1–99:12, July 2010.
 - [8] B. K. Horn. A problem in computer vision: Orienting silicon integrated circuit chips for lead bonding. *Computer Graphics and Image Processing*, 4(3):294 – 303, 1975.
 - [9] R. Kawakami, H. Zhao, R. Tan, and K. Ikeuchi. Camera spectral sensitivity and white balance estimation from sky images. *International Journal of Computer Vision*, 105(3):187–204, 2013.
 - [10] K. Kitagawa. Transparent film thickness measurement by three-wavelength interference method: An extended application of global model fitting algorithm. In *Mechatronics (MECATRONICS), 2012 9th France-Japan 7th Europe-Asia Congress on and Research and Education in Mechatronics (REM), 2012 13th Int'l Workshop on*, pages 94–100, Nov 2012.
 - [11] K. Kitagawa. Thin-film thickness profile measurement by three-wavelength interference color analysis. *Appl. Opt.*, 52(10):1998–2007, Apr 2013.
 - [12] Y. Kobayashi, T. Morimoto, I. Sato, Y. Mukaigawa, and K. Ikeuchi. Reconstructing shape and appearance of thin film objects with hyper spectral sensor. In *Proceedings of the Asian Conference on Computer Vision*, pages 492–506. IEEE Computer Society, 2014.
 - [13] K. W. Meister. Interference spectroscopy. part i. *J. Opt. Soc. Am.*, 31(6):405–426, Jun 1941.
 - [14] D. Miyazaki, M. Kagesawa, and K. Ikeuchi. Determining shapes of transparent objects from two polarization images. In *In IAPR Workshop on Machine Vision Applications*, pages 26–31, 2002.
 - [15] D. Miyazaki, M. Kagesawa, and K. Ikeuchi. Transparent surface modeling from a pair of polarization images. *IEEE Trans. Pattern Analysis and Machine Intelligence*, 26:73–82, 2004.
 - [16] N. J. W. Morris and et al. Reconstructing the surface of inhomogeneous transparent scenes by scatter-trace photography, 2007.

- [17] Y. Mukaigawa, K. Sumino, and Y. Yagi. Rapid brdf measurement using an ellipsoidal mirror and a projector. *Information and Media Technologies*, 4(2):451–462, 2009.
- [18] I. Sadeghi, A. Muñoz, P. Laven, W. Jarosz, F. Seron, D. Gutierrez, and H. W. Jensen. Physically-based simulation of rainbows. *ACM Transactions on Graphics (Presented at SIGGRAPH)*, 31(1):3:1–3:12, Feb. 2012.
- [19] M. Saito, Y. Sato, K. Ikeuchi, and H. Kashiwagi. Measurement of surface orientations of transparent objects by use of polarization in highlight. *J. Opt. Soc. Am. A*, 16(9):2286–2293, Sep 1999.
- [20] Y. Sun, F. Fracchia, M. Drew, and T. Calvert. Rendering iridescent colors of optical disks. In *Rendering Techniques 2000*, Eurographics, pages 341–352. Springer Vienna, 2000.
- [21] Y. Sun, F. D. Fracchia, T. W. Calvert, and M. S. Drew. Deriving spectra from colors and rendering light interference. *IEEE Comput. Graph. Appl.*, 19(4):61–67, July 1999.
- [22] L. Wolff and T. Boult. Constraining object features using a polarization reflectance model. *Pattern Analysis and Machine Intelligence, IEEE Transactions on*, 13(7):635–657, Jul 1991.